Unusual Thermal Polymerization of 1,4-Bis-5-(4,4′-dialkyl-2,2′-bithiazolyl)-1,3-butadiynes: Soluble Polymers from Diacetylenes

Ji-Hoon Lee, M. David Curtis,* and Jeff W. Kampf

Department of Chemistry and the Macromolecular Science and Engineering Center, University of Michigan, Ann Arbor, Michigan 48109-1055

Received July 13, 1999; Revised Manuscript Received January 14, 2000

ABSTRACT: The syntheses of the 1,4-bis-5-(4,4′-dialkyl-2,2′-bithiazole)-1,3-butadiynes, **ABD**s, (**6a**−**c**) are reported. The crystal and molecular structure of the butyl derivative was determined by single-crystal X-ray diffraction. The **BBD** (the 4,4′-di-*n*-butyl **ABD**) molecules are properly aligned in the solid state for topotactic 1,4-polymerization to occur, but these materials do not undergo such polymerization under a variety of conditions. The lack of topotactic polymerization is attributed to the rigidity of the aromatic groups directly bonded to the butadiyne. These compounds do polymerize in the molten state to give soluble polymers that are characterized by UV−vis, FT-IR, and NMR spectroscopies and cyclic voltammetry. Molecular modeling was also used to explore some representative conformation space. These data suggest that the polymerization occurs primarily via 1,2-addition, but some 1,4-addition also occurs.

Introduction

Diacetylenes (**DA**s) $R_1-C\equiv C-C\equiv C-R_2$ are unique in that they form macroscopic monomer single crystals that can be converted into macroscopic polymer single crystals via solid-state polymerization by heat, pressure, and UV or γ-ray irradiation.[1−6] Starting from the pioneering work of Wegner,[7] many papers concerning the synthesis and properties of these polymers have appeared because these materials exhibit electrical transport and nonlinear optical properties.[8−10]

The generally accepted necessary requirement for topotactic polymerization to occur is that the monomer DA molecules pack with their molecular axis at an angle of 45° to the stacking direction and the stacking repeat distance be ≤5 Å, corresponding to a perpendicular distance of 3.5 Å between the molecules. On the basis of our structural studies of 4,4′-dialkyl-2,2′-bithiazole derivatives,[11] we had reason to believe the bithiazole unit would adopt the tilted (or slipped-staircase) stacking motif in a molecule, e.g. **6** (Scheme 1).

Should **6** undergo topotactic polymerization, the stacking of the bithiazole rings along the conjugated backbone could give rise to $\pi-\pi$ interactions in the side groups. Such interactions lead to interesting optical and transport phenomena.[12] We here report the synthesis of **6a**−**c**, their behavior under thermal or photochemical polymerization conditions, and the crystal structure of **6b**.

Experimental Section

Materials. 2-Undecanone (98%), 2-hexanone (98%), bromine (99.5%), urea (99%), chloroacetone (95%, **1a**), dithiooxamide (98%), hexachloro-1,3-butadiene (98%), *n*-butyllithium (2.5 M *n*-hexane solution), and tributyltin chloride (96%) were purchased from Aldrich and used without further purification. Solvents were purified by normal procedures and handled under moisture free atmosphere. All melting points are uncorrected. All reactions of air- and water-sensitive materials were performed under nitrogen. Air- and water-sensitive solutions were transferred with double-ended needles. Column chromatography was performed using silica gel (Selecto Scientific, 63−200 mesh, or Aldrich, 200−400 mesh).

Scheme 1

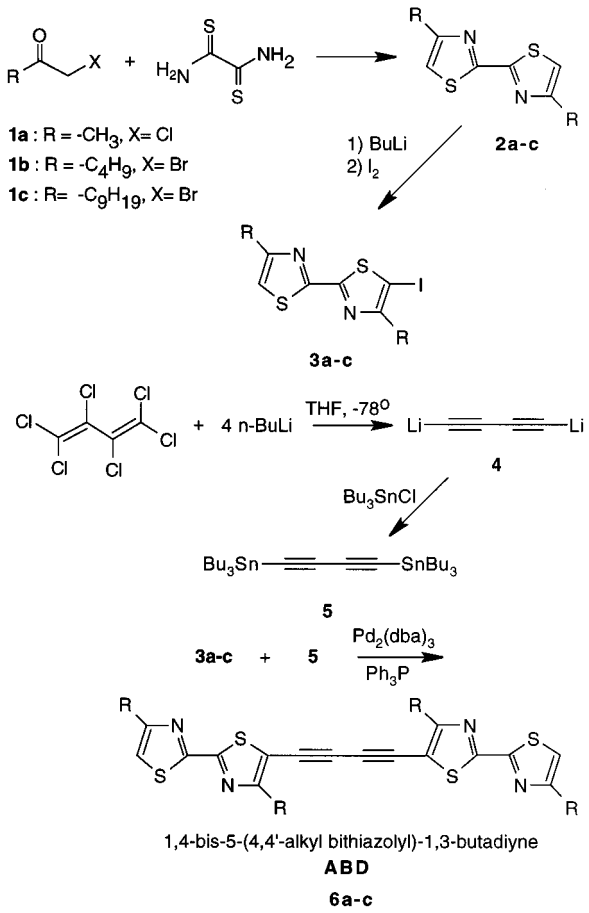

Instruments for Characterization. ^{1}H and ^{13}C NMR spectra were recorded with Bruker AM-360, AM-300, or AM-200 spectrometers, and chemical shifts were referred to the residual proton solvent resonance ($CDCl_3$: 7.26 ppm). Solid-state ^{13}C CPMAS were obtained on a Chemagentics Infinity 400 spectrometer with a 9.4 T wide-bore JMT magnet with resonance frequencies of 100.65 and 400.14 MHz for ^{13}C and ^{1}H, respectively. A 5 mm Zirconia rotor was used for ^{13}C

10.1021/ma9911290 CCC: $19.00
Published on Web 02/19/2000

CPMAS experiments. Samples were spun between 5.3 and 9.3 kHz. Chemical shifts are relative to a tetramethylsilane (TMS) set to 0 ppm for the methyl carbons. A cross polarization contact time of 2.5 ms was used in all CP experiments, with a relaxation delay of 5 s. A 90 ° pulse width of 2.60 μs was used in both ^{1}H and ^{13}C rf channels. FT-IR spectra were measured as KBr pellets on a Nicolet DX-5B or Bomem DA-3 FT-IR spectrometer at a resolution of 2 cm^{-1} . UV−vis spectra were recorded with a Shimadzu UV-3101PC with baseline correction and normalizations carried out using KaleidaGraph software. Electron impact (EI) mass spectra were collected on a VG 70−250-s high resolution spectrometer. Elemental analyses were performed by the University of Michigan Microanalysis Laboratory. Molecular weights and polydispersities of polymers were determined by gel-permeation chromatography (GPC) analysis against polystyrene standards (Waters high-pressure GPC assembly model M590 pump, μ-Styragel columns of 10^5, 10^4, 10^3, 500, and 100 Å, UV detectors, $CHCl_3$ solvent). Differential scanning calorimetry (DSC) and thermogravimetric analyses (TGA) were carried out with a Perkin-Elmer 7 series thermal analyzer under nitrogen atmosphere at heating rates of 20 and 40 °C, respectively. Cyclic voltammograms were obtained with a Princeton Applied Research potentiostat, model 173, interfaced to a PC computer with a program written by Dr. S. Paras, Department of Chemistry, The University of Michigan. The program provides the voltage ramp and handles data collection and manipulation. Solvent was dry acetonitrile, and the supporting electrolyte was tetrabutylammonium tetrafluoroborate (TBAF, 0.1 M). The concentration of the analyte was ca. 4 mM in bithiazole rings. The potentials are referenced vs $Ag/AgNO_3$ (1.3 mM) in 0.1 M Bu_4NPF_6 acetonitrile solution. X-ray diffraction powder data were obtained on a Rigaku Rotaflex diffractometer operated at 40 kV, 100 mA equipped with a Cu target (1.54 Å), and a graphite monochromator. Samples were scanned from 2 to 42° (2θ) at 0.01° intervals and a rate of 1°/min.

Single-Crystal X-ray Structure Determination. A yellow needle of **BBD** was grown by allowing methanol vapor to diffuse into a chloroform solution of the compound. The needle was mounted on a Siemens SMART CCD-based X-ray diffractometer equipped with a normal focus Mo-target X-ray tube (λ = 0.710 73 Å) operated at 2000 W of power (50 kV, 40 mA). The X-ray intensities were measured at 158(2) K with the detector placed at a distance of 5.103 cm from the crystal. A total of 2409 frames were collected with a scan width of 0.3° in ω and an exposure time of 90 s per frame. The frames were integrated with the Siemens SAINT software package with the narrow frame algorithm. The integration of the data using a primitive monoclinic cell yielded a total of 7660 reflections to a maximum 2θ value of 46.62° of which 2579 were independent and 1322 had intensities > $2\sigma(I)$. The final cell constants were based on the *xyz* centroids of 1842 reflections with intensities > $10\sigma(I)$. Analysis of the data showed negligible decay during data collection. The data were not corrected for absorption. The structure was solved and refined with the Siemens SHELXTL (version 5.10) software package in the space group $P2_1/n$ with $Z = 2$ for the formula unit $C_{32}H_{38}N_4S_4$. All non-hydrogen atoms were refined anisotropically. Hydrogen atoms were located on a difference Fourier map and were refined isotropically. The final full matrix refinement based on F^2 converged at R1 = 0.0588 and wR2 = 0.0939 (based on observed data) and R1 = 0.1252 and wR2 = 0.1154 (based on all data). The largest peak (hole) in the final difference map was +0.27 (−0.26) electron/Å^3.

Tables 1−3 contain the crystal and refinement data, the atomic coordinates, and the bond distances and angles. The anisotropic temperature factors and the H atom coordinates are given in the Supporting Information (Tables S1 and S2, respectively).

Synthesis of α-Halomethyl Ketones (1b and 1c). These compounds were synthesized according to a previously reported procedure.[11] The procedures are illustrated in Scheme 1.

1-Bromo-2-hexanone (1b). Yield: 63%. Bp: 40 °C/0.05 mmHg. ^{1}H NMR ($CDCl_3$): δ 0.86 (t, 3H, $-CH_3$), 1.26 (sextet, 2H, $-CH_2-$), 1.51 (quintet, 2H, $-CH_2-$), 2.58 (t, 2H, $-CH_2-$), 3.83 (s, 2H, $-CH_2Br$).

1-Bromo-2-undecanone (1c). Yield: 53%. Mp: 43−43.5 °C. ^{1}H NMR ($CDCl_3$): δ 0.83 (t, 3H, $-CH_3$), 1.25 [m, 12H, $-(CH_2)_6-$], 1.55 (quintet, 2H, β-CH_2-), 2.60 (t, 2H, α-CH_2-), 3.84 (s, 2H, $-CH_2Br$).

Synthesis of 4,4′-Dialkyl-2,2′-bithiazole (ABT, 2a−c). These compounds were synthesized by the method described in the literature.[11] A typical synthetic procedure was as follows: in a 100 mL three-neck round flask equipped with a reflux condenser, nitrogen outlet, and septa were placed 1-bromo-2-undecanone (15.03 mmol), dithiooxamide (7.52 mmol), and EtOH (50 mL); the mixture was heated to reflux. After 30 min of heating, the mixture dissolved to give a bright orange solution that darkened gradually to a deep burgundy color. After 4 h of reflux, the solution was slowly cooled to room temperature and then was allowed to stand in the refrigerator

Table 1. Crystal and Structure Refinement Data for 6b

empirical formula	$C_{32}H_{38}N_4S_4$
fw	606.90
temp, K	158(2)
wavelength, Å	0.71073
cryst syst	monoclinic
space group	$P2_1/n$
unit cell dimens	
a, Å	13.7879(11)
b, Å	5.1900(4)
c, Å	22.585(2)
α, deg	90
β, deg	100.926(2)
γ, deg	90
vol, Å^3; Z	1586.8(2); 2
density (calcd), Mg/m^3	1.270
abs coeff, mm^{-1}	0.327
F(000)	644
cryst size, mm	0.40 × 0.06 × 0.01
θ range for data collcn, deg	1.61−23.27
limiting indices	$-14 \le h \le +15$ $-5 \le k \le +5$ $-14 \le l \le +25$
no. of reflcns collcd	7186
no. of indep reflcns	2287 [R(int) = 0.1026]
abs corr	none
refinement method	full-matrix least-squares on F^2
data/restraints/params	2252/0/259
goodness-of-fit on F^2	1.008
final R indices [$I > 2\sigma(I)$]	R1 = 0.0588, wR2 = 0.0939
R indices (all data)	R1 = 0.1252, wR2 = 0.1134
largest diff peak and hole, e·Å^{-3}	+0.268 and −0.260

Table 2. Atomic Coordinates (×10^4) and Equivalent Isotropic Displacement Parameters (Å^2 × 10^3) for 6b[a]

	x	y	z	U(eq)
S(1)	−48(1)	5780(2)	1437(1)	33(1)
S(2)	−1777(1)	11716(2)	2140(1)	35(1)
N(1)	−1762(3)	7870(6)	1084(2)	28(1)
N(2)	−49(3)	9743(6)	2433(2)	29(1)
C(1)	−174(3)	975(8)	156(2)	30(1)
C(2)	−467(3)	2695(9)	430(2)	32(1)
C(3)	−782(3)	4704(8)	776(2)	26(1)
C(4)	−1660(3)	6035(8)	658(2)	30(1)
C(5)	−2467(4)	5590(11)	124(2)	36(1)
C(6)	−3204(4)	3511(11)	228(2)	40(1)
C(7)	−3791(4)	4201(10)	709(2)	41(1)
C(8)	−4488(5)	2073(12)	809(3)	51(2)
C(9)	−976(3)	7926(8)	1511(2)	27(1)
C(10)	−851(3)	9633(8)	2023(2)	26(1)
C(11)	−1020(4)	12736(9)	2778(2)	32(1)
C(12)	−133(3)	11542(8)	2870(2)	26(1)
C(13)	731(4)	12042(10)	3359(2)	32(1)
C(14)	1482(4)	13874(11)	3171(2)	35(1)
C(15)	2317(4)	14593(13)	3676(3)	45(2)
C(16)	3044(5)	16432(14)	3489(3)	54(2)

[a] U(eq) is defined as one-third of the trace of the orthogonalized $\mathbf{U}_{ij}$ tensor.

Table 3. Bond Lengths (Å) and Angles (deg) for 6b

Bond Lengths			
S(1)−C(9)	1.728(4)	C(3)−C(4)	1.376(6)
S(1)−C(3)	1.729(4)	C(4)−C(5)	1.495(6)
S(2)−C(11)	1.697(5)	C(5)−C(6)	1.530(7)
S(2)−C(10)	1.730(4)	C(6)−C(7)	1.516(7)
N(1)−C(9)	1.307(5)	C(7)−C(8)	1.509(7)
N(1)−C(4)	1.379(5)	C(9)−C(10)	1.441(6)
N(2)−C(10)	1.301(5)	C(11)−C(12)	1.351(6)
N(2)−C(12)	1.379(5)	C(12)−C(13)	1.487(6)
C(1)−C(2)	1.199(5)	C(13)−C(14)	1.523(7)
C(1)−C(1A)[a]	1.372(9)	C(14)−C(15)	1.506(7)
C(2)−C(3)	1.420(6)	C(15)−C(16)	1.503(8)
Bond Angles			
C(9)−S(1)−C(3)	88.2(2)	C(8)−C(7)−C(6)	112.1(5)
C(11)−S(2)−C(10)	88.4(2)	N(1)−C(9)−C(10)	124.2(4)
C(9)−N(1)−C(4)	110.5(4)	N(1)−C(9)−S(1)	116.1(3)
C(10)−N(2)−C(12)	111.2(4)	C(10)−C(9)−S(1)	119.7(3)
C(2)−C(1)−C(1A)	179.2(6)	N(2)−C(10)−C(9)	123.6(4)
C(1)−C(2)−C(3)	177.5(5)	N(2)−C(10)−S(2)	114.7(3)
C(4)−C(3)−C(2)	127.7(4)	C(9)−C(10)−S(2)	121.8(3)
C(4)−C(3)−S(1)	110.8(3)	C(12)−C(11)−S(2)	112.3(4)
C(2)−C(3)−S(1)	121.5(4)	C(11)−C(12)−N(2)	113.5(4)
C(3)−C(4)−N(1)	114.4(4)	C(11)−C(12)−C(13)	127.4(4)
C(3)−C(4)−C(5)	124.9(4)	N(2)−C(12)−C(13)	119.0(4)
N(1)−C(4)−C(5)	120.7(4)	C(12)−C(13)−C(14)	113.2(4)
C(4)−C(5)−C(6)	113.5(4)	C(15)−C(14)−C(13)	114.0(4)
C(7)−C(6)−C(5)	113.8(4)	C(16)−C(15)−C(14)	113.6(5)

[a] Symmetry transformations used to generate equivalent atoms: (A) $-x, -y, -z$.

overnight. The resulting tan solid was collected via filtration, washed with chilled MeOH, and dried in vacuo for 5 h. The solid was further purified by recrystallization.

4,4′-Dimethyl-2,2′-bithiazole (MBT, 2a). The product was recrystallized from *n*-hexane/acetone to yield brownish yellow crystals. Yield: 76%. Mp: 132−133 °C. ^{1}H NMR ($CDCl_3$): δ 2.44 (s, 3H, $-CH_3$), 6.91 (s, 1H); ^{13}C NMR ($CHCl_3$): δ 160.6, 154.0, 115.3, 17.0. UV−vis ($CHCl_3$): λ_{max} = 333 nm.

4,4′-Dibutyl-2,2′-bithiazole (BBT, 2b). The product was recrystallized from methanol/chloroform to yield brownish yellow crystals. Yield: 60%. Mp: 65 °C. ^{1}H NMR ($CDCl_3$): δ 0.93 (t, J = 7.3 Hz, 3H, $-CH_3$), 1.40 [sextet, J = 7.4 Hz, 2H, $-CH_2-$], 1.69 (quintet, J = 7.4 Hz, 2H, β-CH_2-), 2.80 (t, J = 7.7 Hz, 2H, α-CH_2-), 6.93 (s, 1H); ^{13}C NMR ($CDCl_3$): δ 160.8, 159.1, 114.5, 31.2, 31.1, 22.3, 13.8. UV−vis ($CHCl_3$): λ_{max} = 334 nm.

4,4′-Dinonyl-2,2′-bithiazole (NBT, 2c). The product was recrystallized from ethanol to yield brownish yellow crystals. Yield: 73%. Mp: 59−61 °C. ^{1}H NMR ($CDCl_3$): δ 0.88 (t, J = 6.5 Hz, 3H, $-CH_3$), 1.24−1.31 [m, 12H, $-(CH_2)_6-$], 1.73 (m, 2H, β-CH_2-), 2.81 (t, J = 7.7 Hz, 2H, α-CH_2-), 6.92 (s, 1H). ^{13}C NMR ($CDCl_3$): δ 160.1, 158.7, 115.1, 31.8, 31.2, 29.5, 29.4, 29.3, 29.1, 22.6, 18.3, 14.0. UV−vis ($CHCl_3$): λ_{max} = 333 nm.

Synthesis of 5-Iodo-4,4′-dialkyl-2,2′-bithiazole (ABT-I, 3a−c) A typical synthetic procedure was as fellows: in a 250 mL Schlenk flask were placed **2c** (3.3 g, 7.84 mmol) and THF (120 mL) under N_2. The flask was cooled to −78 °C, causing the precipitation of some of the NBT. With stirring, the *n*-BuLi (3.6 mL, 9.02 mmol, 2.5 M hexane solution) was added dropwise, causing a lightening of the yellow color. After 1 h of stirring at −78 °C, the mixture was warmed to room temperature and stirred additionally for 3 h. After the mixture was recooled to −78 °C, I_2 (2.39 g, 9.41 mmol) was added, and the system was allowed to slowly warm to room temperature and stirred for 12 h. Most of the solvent is evaporated under reduced pressure to give a dark red-orange oil. Water (150 mL) was added to the flask. The organics were extracted with $CHCl_3$ (3 × 40 mL) and washed with water (2 × 100 mL), NaCl (saturated, 70 mL), and $NaHSO_4$ (aqueous, 100 mL), and dried over $MgSO_4$ with activated carbon. The product was further purified by silica gel column chromatography (eluent, ethyl acetate:*n*-hexane = 1:5).

5-Iodo-4,4′-dimethyl-2,2′-bithiazole (MBT-I, 3a). Yield: 80%. Mp: 128−130 °C. ^{1}H NMR ($CDCl_3$): δ 2.49 (d, 6H, $-CH_3$), 6.96 (s, 1H). ^{13}C NMR ($CDCl_3$): δ 165.0, 159.9, 158.1, 154.4, 115.7, 71.1, 17.6, 17.1. Mass spectrum *m/e* calcd for $C_8H_7N_2IS_2$ (EI 70 eV): 322, $[M]^+$ base peak.

5-Iodo-4,4′-dibutyl-2,2′-bithiazole (BBT-I, 3b). Yield: 69%, viscous yellow oil. ^{1}H NMR ($CDCl_3$): δ 0.94 (overlapping triplets, 6H, $-CH_3$), 1.42 [m, 4H, $-CH_2-$], 1.69 (m, 4H, β-CH_2-), 2.81 (t, J = 7.7 Hz, 4H, α-CH_2-), 6.94 (s, 1H). ^{13}C NMR ($CDCl_3$): δ 165.3, 162.0, 159.9, 159.3, 114.8, 70.7, 31.2, 31.1, 22.3, 13.9. Mass spectrum *m/e* calcd for $C_{14}H_{19}N_2IS_2$ (EI 70 eV): 406, $[M]^+$ base peak.

5-Iodo-4,4′-dinonyl-2,2′-bithiazole (NBT-I, 3c). Yield: 61%. Mp: 39−43 °C. ^{1}H NMR ($CHCl_3$): δ 0.88 (overlapping triplets, 6H, $-CH_3$), 1.24−1.31 [m, 24H, $-(CH_2)_6-$], 1.73 (m, 4H, β-CH_2-), 2.81 (t, J = 7.7 Hz, 4H, α-CH_2-), 6.94 (s, 1H). ^{13}C NMR ($CHCl_3$): δ 165.4, 162.3, 159.4, 159.2, 114.8, 70.7, 31.9, 31.5, 29.5, 29.4, 29.3, 29.1, 29.0, 22.7, 14.1. Mass spectrum *m/e* calcd for $C_{24}H_{39}N_2IS_2$ (EI 70 eV): 547, $[M]^+$ base peak.

Synthesis of 1,4-Dilithio-1,3-butadiyne (4). THF (70 mL) in a 250 mL Schlenk flask was cooled to −78 °C, and *n*-BuLi (42.4 mL of a 2.5 *n*-hexane solution, 0.11 mol) was added via syringe. The mixture was stirred for 15 min. Subsequently, hexachlorobutadiene (3.95 mL, 25.2 mmol) was added dropwise via syringe. After the addition was complete, the cold bath was removed and the mixture was stirred at room temperature for 3 h. The resulting dark brown mixture was used without further treatment.

Synthesis of 1,4-Di(tributylstannyl)-1,3-butadiyne (5). A mixture of **4** (25.2 mmol) in THF/*n*-hexane was cooled again to −78 °C, and $(n\text{-Bu})_3SnCl$ (15.7 mL, 55.4 mmol) was added dropwise over a period of 15 min via syringe. After addition, the solution was allowed to warm to room temperature and stirred overnight. The dark brown mixture was poured into NH_4Cl (saturated, 150 mL) and extracted with ethyl acetate and washed with H_2O (3 × 100 mL). The organics were separated and dried over $MgSO_4$ with activated carbon. The solvent was removed to give a deep yellow liquid which was distilled in vacuo, yielding a colorless to slightly yellow oil. Yield: 53%. Bp: 160 °C/ 0.05 mmHg. ^{1}H NMR ($CDCl_3$): δ 0.89 (t, 9H, $-CH_3$), 1.01 (t, 6H, $SnCH_2$), 1.18−1.41 (m, 6H, $-CH_2-$), 1.45−1.67 (m, 6H, $-CH_2-$). ^{13}C NMR ($CDCl_3$): δ 93.2, 83.9, 29.1, 27.4, 13.8, 11.51. Mass spectrum *m/e* calcd for $C_{28}H_{54}Sn_2$ (EI 70 eV): 628, $[M]^+$, 571, base peak, $[M - C_4H_9]^+$. FT-IR (NaCl, cm^{-1}): 2958, 2927, 2872, 2854, 2037, 1464, 1418, 1377, 1341, 1074, 960, 876, 866.

Synthesis of 1,4-Bis-5-(4,4′-dialkyl-2,2′-bithiazole)-1,3-butadiynes, ABDs, (6a−c). A typical synthetic procedure was as follows: a dry 100 mL Schlenk flask equipped with a stir bar and N_2 inlet/outlet was charged with $Pd_2(dba)_3$ (0.035 g, 0.06 mmol) and triphenylphosphine (0.079 g, 0.30 mmol). Dry toluene (50 mL) was added, and the system was freeze−pump−thawed. The mixture was allowed to warm to room temperature and stirred until the yellow catalyst color was formed. The solution was transferred via cannula to a dry 100 mL Schlenk flask equipped with a stir bar and N_2 inlet/outlet containing **3c** (1.38 g, 2.5 mmol) and **5** (0.75 g, 1.2 mmol), and a condenser was placed on the flask. The reaction mixture was heated to reflux for 18 h, during which time the fluorescence of solution changed from weak violet to green. The mixture was poured into MeOH (250 mL), and an orange powder was precipitated. The product was collected by filtration and dried under vacuum for 12 h and further purified by silica gel column chromatography (eluent, ethyl acetate:*n*-hexane = 1:4).

1,4-Bis 5-(4,4′-dimethyl-2,2′-bithiazolyl)-1,3-butadiyne, MBD, (6a). Yield: 58%. No melting point was observed below 250 °C in air. Anal. Calcd for $C_{20}H_{16}N_4S_4$: C, 54.52; H, 3.66; N, 12.71. Found: C, 54.85; H, 3.38; N, 12.48. ^{1}H NMR ($CDCl_3$): δ 7.03 (s, 1H, proton of thiazole ring), 2.60 (s, 3H, outer CH_3), 2.51 (s, 3H, inner CH_3). MS (EI 70 eV): 438, base peak, $[M]^+$. FT-IR (KBr, cm^{-1}): 2959, 2917, 2870, 2186, 2144, 1497, 1441, 1399, 1370, 977, 878, 752.

1,4-Bis-5-(4,4′-dibutyl-2,2′-bithiazole)-1,3-butadiyne, BBD, (6b) The product was recrystallized from methanol/chloroform to yield yellowish orange crystals**.** Yield: 70%. Mp: 147.5 °C (DSC 20 °C/min). Anal. Calcd for $C_{32}H_{38}N_4S_4$:

C, 63.33; H, 6.31; N, 9.23. Found: C, 63.28; H, 6.29; N, 9.17. ^{1}H NMR ($CDCl_3$): δ 7.01 (s, 1H, proton of thiazole ring), 2.91 (t, 2H, outer αCH_2), 2.82 (t, 2H, inner α-CH_2), 1.75 (m, 4H, β-CH_2), 1.42 (m, 4H, $-CH_2-$), 0.97 (overlapping triplets, 6H, CH_3-). ^{13}C NMR ($CDCl_3$): δ 166.3, 160.7, 159.9, 159.7, 115.8, 113.6, 82.7, 75.6, 31.3, 30.6, 22.3, 13.9. MS (EI 70 eV): 606, $[M]^+$, base peak; 564, $[M - C_3H_7]^+$. FT-IR (KBr, cm^{-1}): 3112, 2958, 2931, 2870, 2861, 2189, 2141, 1493, 1468, 1399, 1378, 1261, 1103, 977, 880, 739.

1,4-Bis-5-(4,4′-dinonyl-2,2′-bithiazole)-1,3-butadiyne, NBD, (6c). Yield: 71%. Mp: 92.6 °C (DSC 20 °C/min). Anal. Calcd for $C_{52}H_{78}N_4S_4$: C, 70.38; H, 8.86; N, 6.31. Found: C, 68.27; H, 8.68; N, 5.58. ^{1}H NMR ($CDCl_3$): δ 7.01 (s, 1H, proton of thiazole ring), 2.90 (t, 2H, outer α-CH_2), 2.81 (t, 2H, inner α-CH_2), 1.74 (m, 4H, β-CH_2), 1.26 (m, 24H, $-(CH_2)_6-$), 0.88 (overlapping triplets, 6H, CH_3-). ^{13}C NMR ($CDCl_3$): δ 166.3, 160.7, 159.9, 159.8, 116.0, 113.8, 83.0, 75.6, 31.9, 31.5, 30.1, 29.5, 29.4, 29.3, 22.7, 14.1. MS (EI 70 eV): 887, $[M]^+$ base peak. FT-IR (KBr, cm^{-1}): 2958, 2920, 2852, 2192, 2141, 1498, 1468, 1396, 1263, 1026, 876, 805, 739, 719, 701.

Attempted Solid-State Polymerization of BBD by UV Light or Thermolysis. Polymerization by UV light was attempted with samples of three types: a single crystalline sample, a microcrystalline sample dispersed in KBr pellets, and a vacuum-deposited thin film of monomer crystals on quartz. In the photolysis experiments, the samples were exposed to 254 or 366 nm UV light with a sample−source distance of approximately 2−4 cm. A $CuSO_4$ solution was placed between the source and sample to minimize heating from the lamp. Under a N_2 atmosphere, photobleaching of the ABT chromophore was observed. Initially, the UV spectra of the photolyzed materials became nearly identical to those of the thermally polymerized samples (see below); however, the photolyzed materials were insoluble, indicating that cross-linking had occurred under photolytic conditions. Because of their insolubility, these materials could not be further characterized. Continued photolysis caused further loss of intensity at longer wavelengths until the spectrum was nearly identical to that of butyl bithiazole. Prolonged photolysis (72 h) caused some photobleaching even of the bithiazole chromophore. No change in the UV absorption spectrum was observed after the samples were held just below the mp for several days under a N_2 atmosphere.

Thermal Polymerization of the ABDs in the Molten-State. The soluble polymers were prepared by heating the monomer samples in the molten state below their thermal decomposition temperatures (235−240 °C for **BBD**) for 1 h. Nitrogen was used as a purge gas to provide an inert atmosphere during the polymerization. As the polymerization proceeded, the viscosity of the monomers in the molten state increased, and the color also changed gradually from orange to dark brown. After 1 h, the resulting polymers were dissolved in chloroform, and the solution was poured into a large excess of methanol. The precipitated polymers were filtered, washed, and then dried in vacuo to give dark brown solids. The yields of the resulting polymers were 80−90%.

Results and Discussion

Synthesis of the Monomers. Scheme 1 describes an overview of the synthesis of 1,4-bis-5-(4,4′-dialkyl-2,2′-bithiazolyl)-1,3-butadiynes, the **ABD**s. The 4,4′-dialkyl-2,2′-bithiazoles (**2a**−**c**) were prepared in moderate yield by the method described in the literature.[11] Monolithiation of **2a**−**c** using *n*-BuLi at −78 °C in THF followed by iodination yielded compounds **3a**−**c**. The reaction of 1,4-dilithio-1,3-butadiyne (**4**) with tri(*n*-butyl)tin chloride gave the product, 4-di(tributylstannyl)-1,3-butadiyne (**5**). The diacetylene-containing bithiazoles, **6a**−**c,** were synthesized by a Stille coupling reaction between monoiodinated bithiazole compounds **3a**−**c** and di(tributylstannyl)-1,3-butadiyne (**5**) in the presence of a Pd catalyst in toluene. Attempts were made to grow X-ray quality crystals of the **ABD**s by varying the temperature and solvent conditions: the **MBD** was too insoluble, and the **NBD** was too waxy for good crystal growth. However, the **BBD** gave good quality crystals that afforded a structure determination.

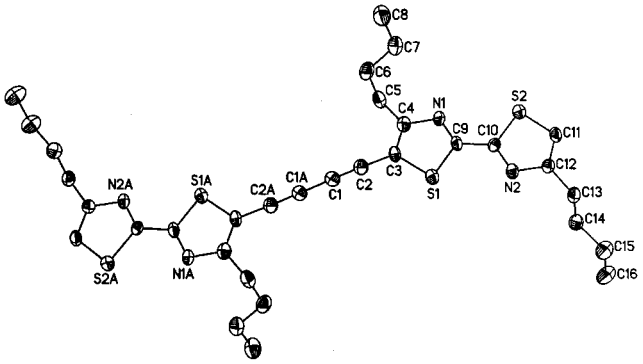

Figure 1. ORTEP drawing with atomic numbering scheme for 1,4-bis-5-(4,4′-dialkyl-2,2′-bithiazolyl)-1,3-butadiyne, **6b**.

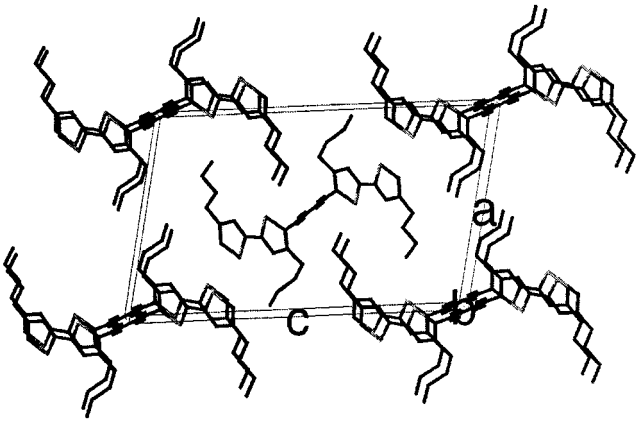

Figure 2. View of the molecular packing of **6b** as seen down the *b* axis of the unit cell.

Crystal Structure of BBD (6b). Figure 1 shows the ORTEP diagram of the molecular structure of **6b** with the atomic numbering scheme. Derived bond distances and angles are in Table 3. The bond distances yield a self-consistent set of radii for $C_{sp_3}-$, $C_{sp_2}-$, $C_{sp}-$, and $N_{sp}-$ single bonds (0.76, 0.74, 0.69, 0.66 Å, respectively); $C_{sp_2}=$ and $N_{sp_2}=$ double bonds (0.68 and 0.62 Å, respectively), and C≡ triple bonds (0.60 Å). These values compare well to the established ones.[13] The only significant variations between observed bond lengths and those calculated with the radii are between C9 and C10 (1.44 Å) vs 1.48 (calculated). The observed shortening may be ascribed to the resonance between the thiazole rings.

The most interesting aspect of the structure concerns the intermolecular packing. In space group $P2_1/n$ with two molecules per unit cell the asymmetric molecular unit consists of half of a molecule. All other atoms are determined by the symmetry operations. Thus, one molecule sits on the inversion center at the corners, and the second molecule lies on the inversion center at the center of the unit cell. Because of the screw axis relationship, these two molecules "tilt" in opposite directions. Figure 2 shows a view of the unit cell down the *b* axis. The molecules at the corners form a "tilted" π-stack, as do the molecules in the center of the cell. Figure 3 is a view at right angles to the *b* axis that shows the two π-stacks edge-on and reveals the opposite tilt angle between the corner stacks and the center

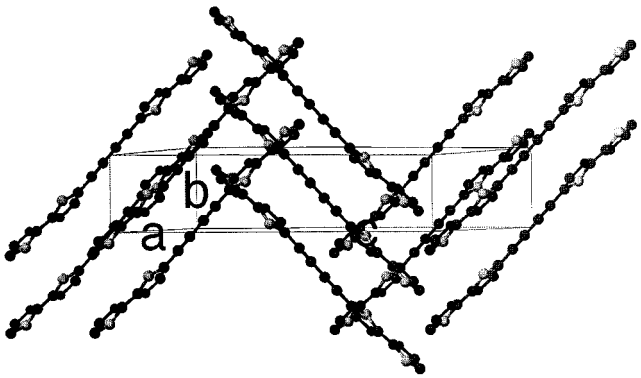

Figure 3. View of the molecular packing of **6b** as seen perpendicular to the *b* axis, showing the 45° angle of the molecules to the stacking axis.

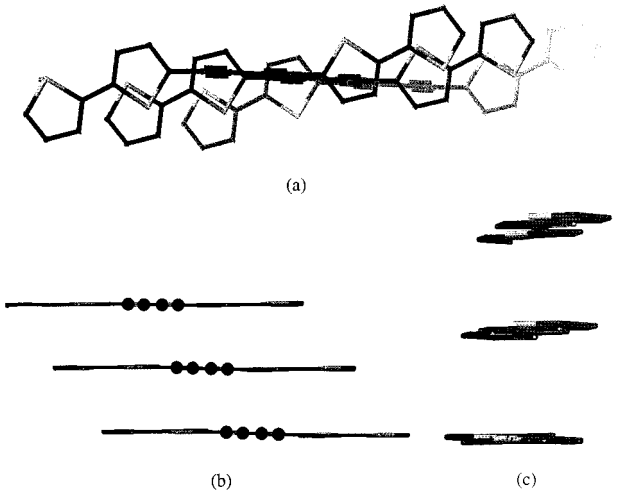

Figure 4. (a) View of slipped π-stack (staircase pattern) as seen perpendicular to the molecular plane, showing the alignment of the diacetylene groups and the minimal overlap between the ring atoms. (b) View orthogonal to that in part a and perpendicular to the long axis of the molecules. (c) View along the long axis of the molecule.

stacks. Figure 4a is a view of a π-stack as seen perpendicular to the molecular plane and shows three molecules lying atop one another in parallel planes, 3.48 Å apart. This view also shows the alignment of the diacetylene cores. Parts b and c of Figure 4 are two views orthogonal to the viewing axis in Figure 4a and show clearly that atom C1 lies directly over atom C4′ of the neighboring molecule so that the C1−C4′ distance is identical to the interplanar distance between the molecules: 3.48 Å.

There are several noteworthy aspects of this packing motif. First, the molecules subtend an angle of 48°with the stacking axis, and the perpendicular distance between the adjacent molecular planes is within the limits required for topotactic polymerization. Second, the tilted π-stack forms a slipped or "staircase" stack that actually *minimizes* $\pi-\pi$ interactions. We have now observed this staircase packing with three alkyl bithiazole dimers,[12] two alkylbithiazoles,[11] and an alkylbis(oxazole),[14] as well as in the polymer, poly(nonylbithiazole).[15] Since direct overlap of filled molecular orbitals (MOs) is repulsive, most simple aromatics, or unsubstituted conjugated oligomers, e.g., sexithiophene, crystallize with the "herringbone" pattern that points the edge ($\delta+$) of one molecule toward the π-system ($\delta-$) of its neighbor. The staircase packing we observe with alkyl-substituted

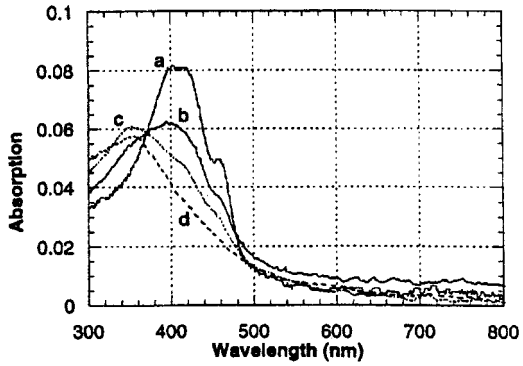

Figure 5. Photobleaching behavior of **BBD** crystal upon UV-irradiation (254 nm) for (a) 2 h, (b) 15 h, (c) 33 h, and (d) 47 h.

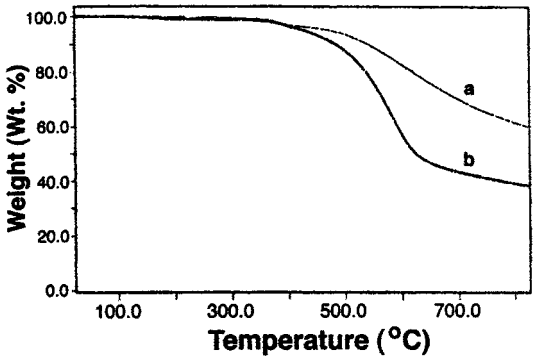

Figure 6. TGA thermograms of (a) **MBD** and (b) **BBD** (40 °C/min under N_2).

oligomers is probably a compromise that allows the side chains to close-pack while minimizing $\pi-\pi$ repulsions. Finally, with two molecules per unit cell, the $\pi-\pi^*$ exciton bands in the solid are split, and the absorption spectra show the fine structure characteristic of $\pi-\pi$ interactions (see ref 12 for a full description of this phenomenon).

Topotactic Polymerization Attempts of BBD in the Solid-State. For the topochemical polymerization of diacetylenes (**DA**s) to occur, the monomer in the crystal must satisfy geometric constraints which include a distance (d) of 5 Å between neighboring monomers measured parallel to the final chain axis and an angle (ϕ) of 45° between the C1−C4 axis and final chain axis.[1−3] As shown above, crystals of BBD satisfy the structural constraints for topotactic **DA** polymerization. However, no polymeric materials were formed via thermal polymerization of crystalline **BBD** or **NBD** at temperatures less than their melting points, nor did UV irradiation in the solid-state give typical **PDA**s that are characterized by long wavelength absorptions (λ_{max} = 500−700 nm). Figure 5 shows the UV−vis absorption behavior of a vacuum-deposited thin film of the **BBD** crystals as a function of irradiation time under nitrogen atmosphere. As the irradiation time increased, the absorption maximum of the **BBD** was observed to blue-shift and become similar to the UV spectra of the thermally polymerized materials (see below, Figure 10). Continued photolysis resulted in gradual bleaching of the characteristic bithiazole absorption at 350 nm, indicating the some degredation of the bithiazole ring system. Although the spectra of the partially photolyzed materials (Figure 5d) were similar to those of the thermal polymers, the photolyzed solids were insoluble, suggesting some cross-linking had occurred. The insolubility precluded further characterization.

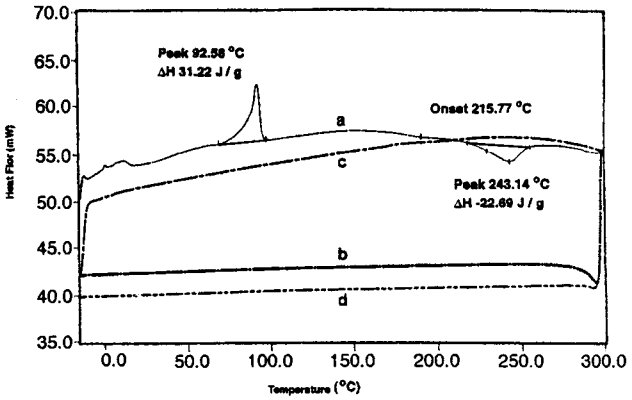

Figure 7. DSC curves of **NBD** at heating rate of 20 °C/min under N_2: (a) first heating, (b) first cooling, (c) second heating, and (d) second cooling.

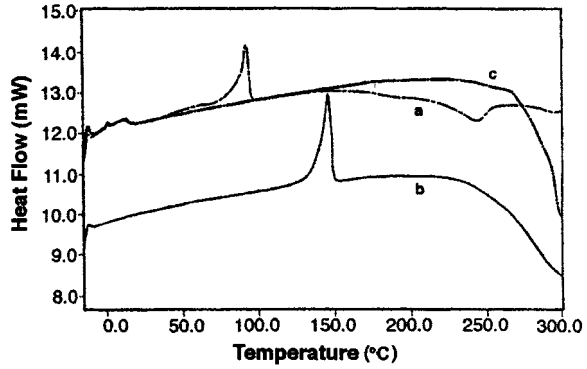

Figure 8. DSC thermograms of (a) **NBD**, (b) **BBD**, and (c) **MBD** (20 °C/min under N_2).

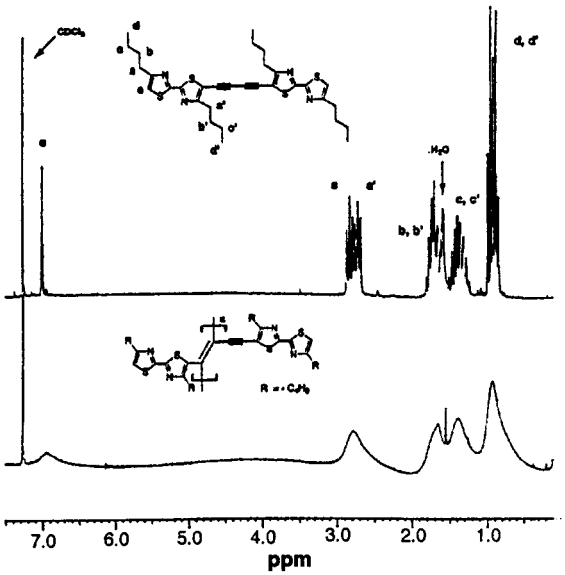

Figure 9. ^{1}H NMR spectra of (a) **BBD** and (b) **PBBD** in $CDCl_3$.

The thermal polymerization of crystals of the **BBD** was attempted at 120 °C, i.e., below the melting point (148 °C) under a nitrogen atmosphere for 7 days. Although there was a color change of the surface of the crystals from yellowish orange to brown, there was no evidence for polymerization based on spectroscopic analysis (UV−vis and FT-IR) of the product (the spectra were identical to starting material). The discoloration appeared to be due to a small amount of surface degradation.

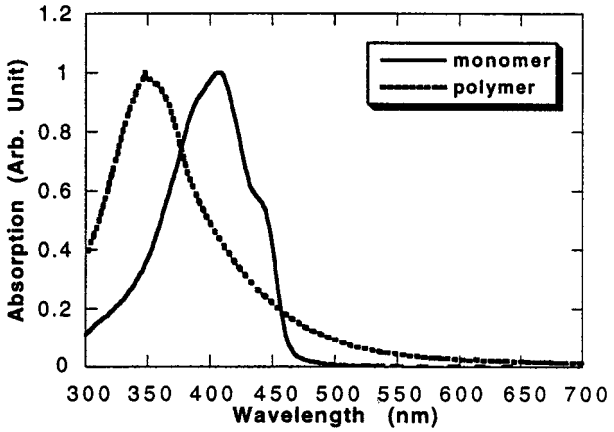

Figure 10. UV−vis absorption spectra of (a) **BBD** and (b) **PBBD** in $CHCl_3$. Intensities were normalized in order to optimally fit the graphs.

Although a few **DA**s with aryl groups directly attached to the diyne moiety are known to undergo topotactic polymerization,[16a] the general lack of reactivity of diaryl diynes has been noted previously.[1,16b] In addition to possible electronic stabilization afforded by direct conjugation of the aryl group to the **DA**, we believe steric hindrance to solid-state polymerization plays an important role. In the **DA** crystal, C1 and C4″ (on the neighboring molecule) are 3.48 Å apart. To form a bond, this distance must decrease to <1.6 Å. There are two ways to decrease the C1···C4″ distance: move two molecules together pairwise, or rotate the molecules in a stack by approximately 30° about an axis perpendicular to both the **DA** and stacking axis. The former method is most likely a high-energy process, but a series of rotations leads to the final polymer geometry and is likely a lower energy, librational motion. When the **DA** is capped by rigid aryl groups, molecule rotation is blocked because an aryl group is pushed into the next molecule before the C1···C4″ distance approaches bonding range. On the other hand, an aryl attached to the **DA** via a methylene group can bend back to allow the rotation to occur. Thus, the rigidity of the **DA**−substituent group may play an important role in the ability of **DA**s to undergo topotactic polymerization.

Thermal Polymerization of the ABDs. The thermal stabilities of the monomers were investigated by thermogravimetric analysis. The thermal decomposition temperatures of the monomers were above 450 °C for the **MBD** and 400 °C for the **BBD**, respectively (Figure 6). Figure 7 shows the DSC thermogram of **NBD**. The endotherm at 93 °C corresponds to the mp. This is followed by an exotherm (10.6 kJ/mol) that has an onset at ca. 216 °C and peaks at 243 °C. Upon cooling, and upon a second heat-cool cycle, the DSC thermogram is featureless. If the heat cycle is stopped and cooling commenced before the onset of the exotherm, then an exotherm corresponding to the crystallization of the melt is observed. Similar behavior was observed with **BBD**, but **MBD** showed no melting peak prior to the exotherm (Figure 8). This observation suggests that the **ABDs** are undergoing a thermal polymerization. **NBD** and **BBD** melt prior to the polymerization, but **MBD** polymerizes before the mp is reached. The onset temperatures (T_p) for polymerization are 266 °C (**MBD**), 236 °C (**BBD**), and 216 °C (**NBD**). It is not clear why the T_p's depend on the length of the alkyl side chain because **BBD** and **NBD** polymerize in the melt. Perhaps the viscosity of

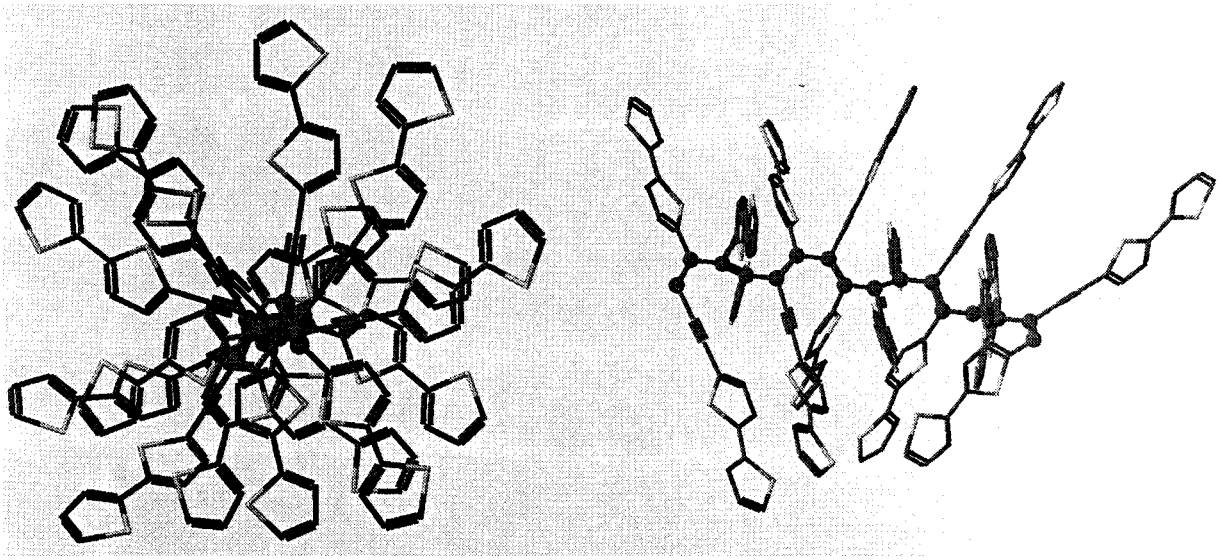

Figure 11. One of many possible chain conformations that results in acceptable distances between the side chain substituents. The alkyl groups have been removed for clarity. Views down the chain axis (left) and at a right angle to the chain axis (right).

the melt is playing a role, and the longer side chain decreases the viscosity by diluting the polar contributions of the thiazole rings.

In general, acetylene compounds are known to easily undergo cross-linking reactions on exposure to heat or irradiation, giving insoluble polymeric materials.[17] However, in the case of the bithiazole-containing **DA**s, the polymers formed by thermal polymerization at temperatures above T_m but below their thermal decomposition temperature (T_d) were completely soluble in common organic solvents such as chloroform, THF, toluene, and so on. This suggests that there are no cross-linking reactions, possibly as a result of the steric bulk of dialkylbithiazole substituents. The GPC of **PBBD** (in $CHCl_3$ vs polystyrene standards)showed a broad, bimodal MW distribution (M_p's $= 1.9 \times 10^5$ and 1.9×10^3) with values, $M_w = 1.9 \times 10^5$ and $M_n = 4.9 \times 10^3$, with PDI = 3.86. Dark brown films of the resulting polymers, obtained by solvent-casting or spin casting on glass slides, were brittle, but the films were amorphous as shown by XRD. The presence of the considerable fraction of low MW material may be responsible for the brittleness of cast films. The polymers were stable toward oxidation by air, and there was no significant change in their UV−vis spectra even after several months. To our best knowledge, there have been no reports of the polymerization of **DA**s in the molten state except for the thermal polymerization of liquid-crystalline **DA**s, in which the molecular weight of the polydiacetylenes was relatively low ($\sim 2.5 \times 10^3$).[18]

The exact chemical structure of the polymers obtained in the molten state was difficult to determine. NMR (^{1}H and ^{13}C NMR) were of limited use due to the number of quaternary carbon atoms. The ^{1}H NMR spectra show only the side chain protons (Figure 9), and the ^{13}C NMR spectra were of low quality (extremely broad, weak, and noisy) due to the relative rigidity of the polymer backbone. On the basis of negative evidence, it is probable that the thermal polymerization in the molten state takes place predominantly through 1,2-addition, or via a mixture of 1,2- and 1,4-additions because spectroscopic data and solubility properties are not consistent with extensive polymerization through 1,4-addition. Generally, 1,4-polymerization of diacetylenes produces polydiacetylenes that are poorly soluble, infusible, highly crystalline, and with absorption maxima in the 500−700 nm region.[1−3] The present polymers possess none of these qualities.

Figure 9 shows the ^{1}H NMR spectra of both the **BBD** and the **PBBD**, whose area ratios coincided well with those for the expected structures**.** It was found that the only significant difference between the NMR spectrum of **BBD** and that of **PBBD** was the broadening of all the peaks in the latter. Similar results were obtained for the polymer derived from **NBD**, but the insolubility of **PMBD** prevented our obtaining NMR data on this polymer. Figure 10 shows the UV−vis absorption spectra of the **BBD** and the **PBBD**. The absorption maximum of the polymer is highly blue-shifted to 348 nm (absorption maximum of the **BBD** and simple 4,4′-dialkyl-2,2′-bithiazoles are 407 and 330 nm, respectively). The polymer also showed a long tail-band extending into the visible region, suggesting some distribution of segments with longer conjugation lengths. The absorption spectra of **PMBD** and **PNBD** were almost identical to that of the **PBBD** in solution or in the solid state, showing that the backbone conformations are independent of the length of alkyl side chain and solid-state packing effects. The remarkable hypsochromic effect is explained by a shortening of the effective conjugation length in the polymers vis-à-vis the monomers. The effective conjugation length of the conjugated double bonds in the polymer backbone is limited by twisting of the chain backbone caused by the steric hindrance between the side-chain substituents. Molecular modeling (CAChe, enhanced MM2 force field) showed that only highly twisted conformations of 1,2-polymers gave acceptable distances between the thiazole rings in the side chains. Figure 11 shows that even with the backbone in a twisted, gauche configuration there is still considerable crowding of the side chain thiazole rings. Conformations which allowed planar, conjugated segments in the 1,2-addition backbone caused inter-ring contacts considerably less than the sum of van der Waals radii (see figures in the Supporting Information). Modeling also showed that conformations resulting from 1,4-additions are considerably less crowded.

The FT-IR spectra of the monomer **BBD** and corresponding one for the **PBBD** are shown in Figure 12 and provide evidence that the bithiazole chromophore re-

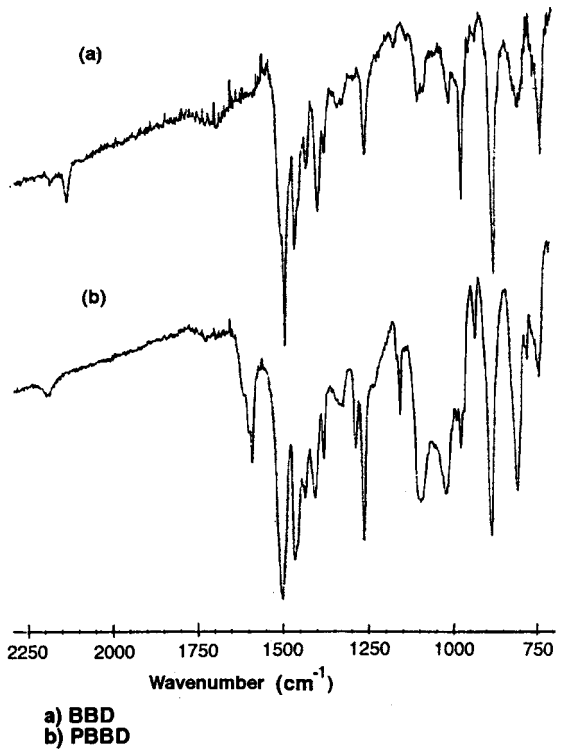

Figure 12. FT-IR spectra of (a) **BBD** and (b) **PBBD** on KBr disk.

mains intact after the polymerization. The monomer spectrum shows two infrared bands at 2190 (asymmetric) and 2139 cm^{-1} (symmetric) whose origin is the stretching vibrational modes of the coupled C−C triple bonds in symmetrically substituted diacetylenes. Only one $\upsilon_{C\equiv C}$ is present at 2197 cm^{-1} in the FT-IR spectrum of the corresponding **PBBD**, suggesting that loss of the molecular symmetry of the monomer takes place during the polymerization. A single, high frequency $\upsilon_{C\equiv C}$ mode has been observed previously in 1,2-polymerized **DA**s.[19] Furthermore, in the spectrum of the **PBBD**, new infrared bands around 1588 cm^{-1}, with two additional shoulders at 1597 and 1613 cm^{-1}, appear as the polymerization proceeds. These bands are attributed to the C═C stretching vibration modes in the newly formed polymer backbone. The two additional small peaks at 1597 and 1613 cm^{-1} probably are due to the interaction between adjacent double bonds in the polymer backbone. In the same region, the monomer does not present any C═C stretching vibrational modes. The frequencies and the assignment of the main characteristic bands of the **BBD** and the **PBBD** are summarized in Table 4. In fact, the formation of these double bonds during the polymerization is also suggested by the solid-state ^{13}C NMR spectrum of the **PBBD**, which, despite its poor quality showed broad, ill-resolved peaks in the range of 123−143 ppm that can be assigned to the vinylic carbons in the conjugated main chain.

Cyclic Voltammetry. Conjugated polymers that contain the bithiazole moiety are capable of being reversibly n-doped to the extent of one electron per bithiazole ring.[20] We therefore studied the cyclic voltammetry of **PBBT**. Figure 13 shows the CV curve vs ferrocene/ferrocenium as internal standard of a thin film of the solid polymer on a glassy carbon electrode.[21] There appear to be three reduction waves: a weak shoulder at −1.5 V, followed by shoulders at −2.0 and −2.2 V. The peaks at −2.0 and −2.2 V are near the

Table 4. Characteristic FT-IR Frequencies (cm^{-1})[a] for the BBD and the PBBD

BBD	PBBD	molecular vibration
2190 w (asymm), 2139 w (symm)	2197 w	C═C str
	1588 m 1597, 1613	C═C str
1495 vs	1500 vs	C═N str
1460 s, 1455 m	1464 s, 1455 s	CH_2 def, CH_3 asymm def
1431 w	1434 m	C═C def (thiazole ring)
1378 w	1378 m	CH_3 symm def
879 vs, 805 m	880 vs, 802 s	Ar C−H out-of-plane bend in thiazole ring
738 m	737 m	CH_2 rock

[a] Intensities: vs = very strong, s = strong, m = medium, w = weak. Abbreviations: asymm, asymmetric, symm, symmetric; str, stretching; def, deformation; bend, bending; rock, rocking.

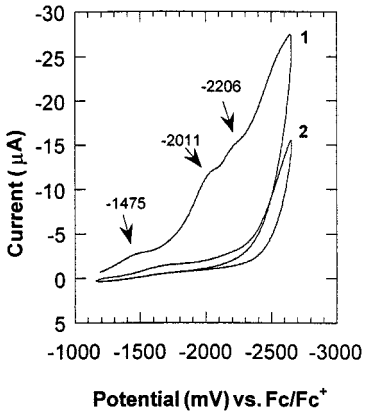

Figure 13. CV (100 mV/s) curve of **PBBD** in acetonitrile vs ferrocene/ferrocenium. Curve 2 is a blank run.

reduction potential of bithiazole monomers. This similarity supports the conclusion drawn from the UV−vis spectra that most of the rings are not conjugated in the polymers. The weak shoulder near −1.5 V, however, suggests the presence of a small amount of conjugated regions, and the species responsible for this reduction activity may be related to the chromophores responsible for the long wavelength tail in the UV−vis spectra of these materials. The second scan, labeled "2" in the Figure, shows that the reduced film dissolved and left the surface. The loss of material from the electrode most likely accounts for the electrochemical irreversibility, since the reduction of the bithiazole groups is known to be reversible.[20a]

Conclusions. DAs directly substituted with rigid aryl groups do not readily undergo topotactic polymerization even when the molecules are properly aligned as in the bithiazole-substituted **DA**s presented here. We believe that the rigidity of the aryl substituents prevent those solid-state rotations of the molecules with respect to one other that bring the diacetylene carbon atoms into bonding range. Thermal polymerization of the soluble **BBD** and **NBD** monomers in the molten state gave soluble polymers that are most likely the result of primarily 1,2-addition with some 1,4-addition. Evidence for this mode of polymerization includes the hypsochromic shift of the UV−vis π-π^* absorption peak, molecular modeling, and the FT-IR and CV behavior.

Acknowledgment. This research was supported by the National Science Foundation (DMR-9510274) and by the University of Michigan Office of the Vice-President for Research materials science initiative.

Supporting Information Available: Crystallographic tables and figures showing UV−vis absorption spectra and space-filling models of **PNBD**. This material is available free of charge via the Internet at http://pubs.acs.org.

References and Notes

(1) (a) Ogawa, T. In *Polymeric Materials Encyclopedia*; Salamone, J. C. Eds.; CRC Press: Boca Raton, FL, 1996; Vol. 8, p 5725. (b) Sandman, D. J. *Ibid*. p 1468. (c) *Crystallographically Ordered Polymers*; Sandman, D. J., Ed.; ACS Symposium Series 337; American Chemical Society: Washington, DC, 1987.

(2) Okada, S.; Naknishi, H.; Matsuda, H. In *Polymeric Materials Encyclopedia*; Salamone, J. C., Eds.; CRC Press: Boca Raton, FL, 1996; Vol. 11, p 8393.

(3) Kricheldorf, H. R.; Schwarz, G. In *Handbook of Polymer Synthesis*; Kricheldorf, H. R., Eds.; Marcel Dekker: New York, 1991; Chapter 27, p 1629.

(4) (a) Shimada, S.; Masaki, A.; Hayamizu, K.; Matsuda, H.; Okada, S.; Nakanishi, H. *Chem. Commun.* **1997**, 1421. (b) Shimada, S.; Masaki, A.; Okada, S.; Nakanishi, H. *Nonlinear Opt.* **1995**, *13*, 1421.

(5) Cuniberti, C.; Dellepiane, G.; Piaggio, P.; Musso, G. F. *Chem. Mater.* **1996**, *8*, 708.

(6) Hammond, P. T.; Rubner, M. F. *Macromolecules* **1997**, *30*, 5773.

(7) Wegner, G. *Z. Naturforsch., B: Anorg. Chem., Org. Chem., Biochem., Biophys., Biol.* **1969**, *24B*, 824.

(8) Liao, J.; Martin, D. C. *Macromolecules* **1996**, *29*, 568.

(9) Masse, C. E.; Vander Wiede, K.; Kim, W. H.; Jiang, X. L.; Kumar, J.; Tripathy, S. K. *Chem. Mater.* **1995**, *7*, 904.

(10) Bassler, H. In *Polydiacetylenes*; Cantow, H. J., Eds.; Springer Verlag: Berlin, 1984; p 1.

(11) (a) Nanos, J. I.; Kampf, J. W.; Curtis, M. D.; Gonzalez, L.; Martin, D. C. *Chem. Mater.* **1995**, *7*, 2232. (b) Politis, J. K.; Curtis, M. D.; Gonzales, L.; Martin, D. C.; He, Y.; Kanicki, J. *Chem. Mater.* **1998**, *10*, 1713.

(12) Koren, A. B.; Curtis, M. D.; Kampf, J. Submitted for publication.

(13) Allen, F. H.; Kennard, O.; Watson, D. G.; Brammer, L.; Orpen, A. G.; Taylor, R. *J. Chem. Soc., Perkin Trans. 2* **1987**, S1.

(14) Politis, J. K.; Somoza, F. B., Jr.; Kampf, J. W.; Curtis, M. D.; González Ronda, L.; Martin, D. C. *Chem. Mater.* **1999**, *11*, 2274.

(15) González Ronda, L.; Martin, D. C.; Nanos, J. I.; Politis, J. K.; Curtis, M. D. *Macromolecules* **1999**, *32*, 4558.

(16) (a) Tokura, Y.; Koda, T.; Itsubo, A.; Miyabayashi, M.; Okuhara, K.; Ueda, A. *J. Chem. Phys.* **1986**, *85*, 99. (b) Wegner, G. *Makromol. Chem.* **1972**, *154*, 35.

(17) Wegner, G. *Makromol. Chem.* **1970**, *134*, 219.

(18) (a) Milburn, G. H. W.; Werninck, A.; Tsibouklis, J.; Bolton, E.; Thomson, G.; Shand, A. J. *Polymer* **1989**, *30*, 1004. (b) Tsibouklis, J.; Werninck, A.; Shand, A.; Milburn, G. H. W. *Liq. Cryst.* **1988**, *3*, 1393. (c) Tsibouklis, J. In *Polymeric Materials Encyclopedia*, Salamone, J. C., Eds.; CRC Press: Boca Raton, FL, 1996; Vol. 5, p 3787.

(19) Barentsen, H. M.; van Dijk, M.; Kimkes, P.; Zuilhof, H.; Sudhölter, E. J. R. *Macromolecules* **1999**, *32*, 1753.

(20) (a) Curtis, M. D.; Cheng, H.; Johnson, J. A.; Nanos, J. I. *Chem. Mater.* **1998**, *10*, 13. (b) Yamamoto, T.; Suganuma, H.; Maruyama, T.; Inoue, T.; Muramatsu, Y.; Arai, M.; Komarudin, D.; Ooba, N.; Tomaru, S.; Sasaki, S.; Kubota, K. *Chem. Mater.* **1997**, *9*, 1217.

(21) The reported potentials are vs the ferrocene/ferrocenium (Fc/Fc^+) couple, obtained by adding a crystal of ferrocene to the solution. The Fc/Fc^+ couple has a potential of +400 mV vs the NHE: Koepp, H. M.; Wendt, H.; Strahlow, H. *Z. Elektrochem. 1960*, *64*, 483.

MA9911290